

Coordination of Frequency and Load Resistor to Improve Efficiency of Wireless Power Transfer System Under Frequency Drift

Zhongqi Li^{1, 2}, Wangyang Cheng¹, Jiliang Yi^{1, *}, and Junjun Li¹

Abstract—Magnetic resonant wireless power transfer (WPT) is an emerging technology that may create new applications for wireless power charging. However, low efficiency resulting from resonant frequency drift is a main obstructing factor for promoting this technology. In this paper, a novel method of coordinating the operating frequency and load resistor is proposed to prevent frequency drift. The system efficiency and input impedance are obtained by solving the system equivalent equations. In addition, the new resonant frequencies can be obtained by solving the input impedance equations. Moreover, the process of the coordination method is illustrated. When resonant frequency drift occurs, the system can now operate at the resonant state, and the efficiency can be improved by using the proposed method. The WPT system via magnetic resonance coupling is designed. Simulated and experimental results validating the proposed method are given.

1. INTRODUCTION

Wireless power transfer (WPT) methods are receiving increasing attention in the international research community [1, 2]. A new wireless power transfer technology based on strongly coupled magnetic resonances is proposed [3–5]. This technology is used widely in the fields of medical devices, charging of mobile and electric vehicles [6–8]. One of the most important problems is to improve efficiency in magnetic resonant wireless power transfer system [3–5].

There are many researches in the WPT system in order to obtain high transfer efficiency. The first approach is to optimize the circuit topologies [9–11]. The circuit topological structure of the series-shunt mixed-resonant is proposed to obtain high efficiency [9]. The second approach is to use novel system structures, such as a three-coil structure [12–14], a novel four-coil structure and a multiple-coil structure [15–18]. The third approach is to optimize the parameters of resonant coil [19, 20]. Finally, the optimization methods are used to improve the efficiency, such as optimizing the operating frequency [21], optimizing coupling coefficients [22, 23] and the impedance matching method [24–27]. However, these methods are analyzed in the WPT system under the condition of working at the resonant state.

The condition of working at the resonant state is rather difficult to be satisfied in practical applications because some reasons may result in the resonant frequency drift as follows: (1) inductance or capacitance of the coil may change easily affected by external environment changes, and resonant frequency drift will then occur; (2) Some materials (such as aluminum foil, styrofoam, and humans) may alter the inductance or capacitance of the resonant coil [3], and resonant frequency drift may occur; (3) The error between the nominal value of the capacitor and the actual value of the capacitor may result in resonant frequency drift; (4) the capacitance of the resonant coil may be changed with the variations of temperature, the resonant frequency is also changed as the the capacitance of the resonant coil is changed. The efficiency will drastically decrease when resonant frequency drift occurs. In order to

Received 15 October 2018, Accepted 21 November 2018, Scheduled 3 December 2018

* Corresponding author: Jiliang Yi (iee.china@126.com).

¹ College of Traffic Engineering, Hunan University of Technology, Zhuzhou 412007, China. ² College of Electrical and Information Engineering, Hunan University, Changsha 410082, China.

maintain the required resonant state, the resonant frequency of each coil is adjusted manually by using the external compensating capacitance when the external environment is changed. However, the WPT system may have several resonant coils in practical applications [28]. It is impractical for the WPT system to manually adjust the external compensating capacitance of each coil in practical applications. A frequency-tuned wireless charging system is proposed and successfully demonstrated to enhance the power transfer efficiency [26]. However, it is not considered that the resonant frequencies are changed with the load resistor variations. In this paper, a method of coordinating the operating frequency and load resistor is proposed. It is found that there may be multiple resonant frequencies for different load resistors. The efficiency is the highest at the optimum resonant frequency. When resonant frequency drift occurs, the optimum resonant frequency may be obtained by using the proposed method. Then the system may operate at the resonant state and the optimum efficiency may be obtained.

The rest of the paper is organized as follows. Section 2 establishes the system model and theory. Section 3 analyzes the efficiency with only adjusting the operating frequency. Section 4 analyzes the proposed efficiency improvement method. Section 5 presents the experimental setup and measurement results. Section 6 concludes this paper.

2. MODEL AND THEORETICAL ANALYSIS

The WPT system is composed of two resonant coils: transmission and receiving resonant coils, labeled as Tx and Rx, as shown in Fig. 1. D is the distance between Tx and Rx, C_{Tx} the external compensating capacitance of Tx, and C_{Rx} the external compensating capacitance of Rx. The WPT system can be represented in terms of lumped circuit elements (L , C , and R), as shown in Fig. 2. V_s is the source power, R_1 the parasitic resistor of Tx, R_2 the parasitic resistor of Rx, R_s the internal resistor of the power source, R_L the load resistor, L_1 the inductance of Tx, L_2 the inductance of Rx, M the mutual inductance between Tx and Rx, Z_{in} the input impedance, ω_1 the angular frequency of Tx, ω_2 the angular frequency of Rx, and ω_0 the original resonant angular frequency of each coil. All angular frequencies are shown in Table 1.

Table 1. Angular frequencies.

Symbol	Quantity	Definition
ω	The operating angular frequency	$2 \times \pi \times f$ $0.6f_0 < f < 1.4f_0$
ω_0	The original resonant angular frequency	$2 \times \pi \times f_0$ ($f_0 = 100$ kHz)
ω_1	The angular frequency of the transmission coil	$\omega_1 = (L_1 C_1)^{-1/2}$
ω_2	The angular frequency of the receiving coil	$\omega_2 = (L_2 C_2)^{-1/2}$
ω_{RES-m} ($m = 1, 2, 3$)	The new resonant angular frequency with frequency drift	$\omega_{RES-1}, \omega_{RES-2}$ ω_{RES-3}
ω_{RES}	ω_{RES} is the resonant frequency corresponding to the optimal efficiency	ω_{RES}

By applying Kirchhoff's voltage law (KVL), the WPT system is presented as follows:

$$\begin{cases} Z_1 I_1 + j\omega M I_2 = V_s \\ j\omega M I_1 + Z_2 I_2 = 0 \end{cases} \quad (1)$$

$$\begin{cases} Z_1 = R_S + R_1 + j\omega L_1 + 1/(j\omega C_{Tx}) \\ Z_2 = R_L + R_2 + j\omega L_2 + 1/(j\omega C_{Rx}) \end{cases} \quad (2)$$

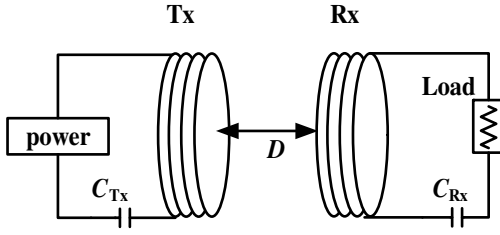


Figure 1. The simplified schematic of the WPT system based on magnetically coupling resonator.

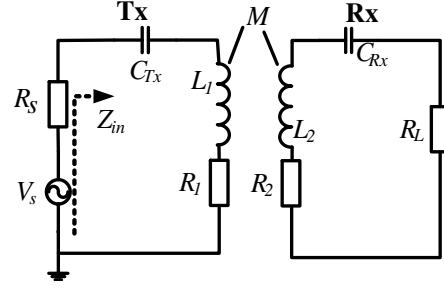


Figure 2. The equivalent circuit model for the WPT system. Each coil is modeled as series resonators.

where I_1 is the current of Tx, I_2 the current of Rx, and ω the operating angular frequency.

The expressions of I_1 and I_2 can be obtained by solving Eqs. (1) and (2).

$$\begin{cases} I_1 = \frac{V_s Z_2}{Z_1 Z_2 + (\omega M)^2} \\ I_2 = -\frac{j\omega M V_s}{Z_1 Z_2 + (\omega M)^2} \end{cases} \quad (3)$$

The expression of efficiency in Eq. (4) is as follows:

$$\eta = \left| \frac{I_2^2 R_L}{V_s I_1} \right| = \left| \frac{(\omega M)^2 R_L}{Z_1 Z_2^2 + (\omega M)^2 Z_2} \right| \quad (4)$$

Equation (2) is substituted into Equation (4). Then the expression of efficiency in Equation (5) can be obtained.

$$\eta = \left| \frac{I_2^2 R_L}{V_s I_1} \right| = \left| \frac{U^2 U_L}{\{(1 + U_s + j\varepsilon_1 Q_1)(1 + U_L + j\varepsilon_2 Q_2)\}^2 + (1 + U_L + j\varepsilon_2 Q_2)U^2} \right| \quad (5)$$

where the source matching factor is defined as $U_s = R_s/R_1$, the load matching factor defined as $U_L = R_L/R_2$, the strong-coupling parameter defined as $U = \omega M/(R_1 R_2)^{1/2}$, the unload quality factor of Tx defined as $Q_1 = \omega L_1/R_1$, the unload quality factor of Rx defined as $Q_2 = \omega L_2/R_2$, the angular frequency deviation factor of Tx defined as $\xi_1 = 1 - \omega_1^2/\omega^2$, and the angular frequency deviation factor of Rx defined as $\xi_2 = 1 - \omega_2^2/\omega^2$.

The input impedance can be defined by Eq. (6)

$$Z_{in} = V_s/I_1 - R_s \quad (6)$$

Equation (2) is substituted into Eq. (6). Then the expression of the input impedance can be obtained as follows:

$$Z_{in} = R_1 \frac{\{(U^2 + (1 + U_s)(1 + U_L) - Q_1 Q_2 \varepsilon_1 \varepsilon_2) + j(Q_1 \varepsilon_1 (1 + U_L) + Q_2 \varepsilon_2 (1 + U_s))\}((1 + U_L) - jQ_2 \varepsilon_2)}{(1 + U_L)^2 + Q_2^2 \varepsilon_2^2} - R_s \quad (7)$$

Equation (7) can be simplified into Eq. (8)

$$Z_{in} = R_1 \frac{\{(1 + U_L)^2 + U^2(1 + U_L) + Q_2^2 \varepsilon_2^2\} + j[(1 + U_L)^2 Q_1 \varepsilon_1 + Q_1 \varepsilon_1 Q_2^2 \varepsilon_2^2 - U^2 Q_2^2 \varepsilon_2^2]}{(1 + U_L)^2 + Q_2^2 \varepsilon_2^2} \quad (8)$$

According to Eq. (8), the input impedance characteristic angle (θ) between V_s and I_1 can be obtained as follows:

$$\begin{aligned} \theta &= \arctan(\text{Im}(Z_{in})/\text{Re}(Z_{in})) \\ &= \arctan\left(\frac{(1 + U_L)^2 Q_1 \varepsilon_1 + Q_1 Q_2^2 \varepsilon_1 \varepsilon_2^2 - U^2 Q_2^2 \varepsilon_2^2}{(1 + U_L)^2 + U^2(1 + U_L) + Q_2^2 \varepsilon_2^2}\right) \end{aligned} \quad (9)$$

where $\text{Re}(Z_{in})$ is the real component of Z_{in} , and $\text{Im}(Z_{in})$ is the imaginary component of Z_{in} . θ is the input impedance characteristic angle. When $\theta = 0$, the impedance is purely resistive, and Eq. (10) can be obtained from Eq. (9).

$$\begin{aligned} & (L_1 L_2^2 - L_2 M^2) \omega^6 + [(R_2 + R_L)^2 L_1 - 2L_1 L_2^2 \omega_2^2 - L_1 L_2^2 \omega_1^2 + L_2 M^2 \omega_2^2] \omega^4 \\ & + [L_1 L_2^2 \omega_2^4 + 2L_1 L_2^2 \omega_1^2 \omega_2^2 - (R_2 + R_L)^2 L_1 \omega_1^2] \omega^2 - L_1 L_2^2 \omega_1^2 \omega_2^4 = 0 \end{aligned} \quad (10)$$

The resonant angular frequencies can be obtained by solving Eq. (10). The resonant angular frequencies ω_{RES_m} ($m = 1, 2, 3$) are dependent on the angular frequency of the transmission resonant coil ω_1 , the angular frequency of the receiving resonant coil ω_2 , and the load resistor R_L when the parameters of each resonant coil and the transfer distance D are given. According to Eq. (5), the efficiency is also dependent on the resonant angular frequencies ω_{RES_m} and the load resistor R_L .

3. ANALYSIS OF ADJUSTING FREQUENCY METHOD

In this section, the efficiency can be improved by using the method of adjusting the operating frequency. When resonant frequency drift occurs and the load resistor is fixed at 50Ω , according to (9), θ becomes greater than zero at $\omega = \omega_0$ and the efficiency is reduced according to Eq. (5). Fig. 3(b) shows efficiency versus ω/ω_0 profiles for different combinations of ω_1 and ω_2 . It may be observed that the efficiency is 4.1% with $\omega_1 = 0.8\omega_0$, $\omega_2 = 1.2\omega_0$, and $\omega = \omega_0$, and the efficiency is 3.4% with $\omega_1 = 1.2\omega_0$, $\omega_2 = 0.8\omega_0$, and $\omega = \omega_0$. This has clearly shown that when the resonant frequency of the two resonant coils drifts away (due to e.g., parameters variation), working at the original resonant frequency will no longer result in high efficiency. This is because θ is no longer close to zero degree (close to plus/minus 90 degrees instead) at the original resonant angular frequency, as may be observed from Fig. 3(a). The circuit is no longer resistive, and the energy tends to be stored in the inductance/capacitance instead of being transferred away, resulting in a low power transfer efficiency.

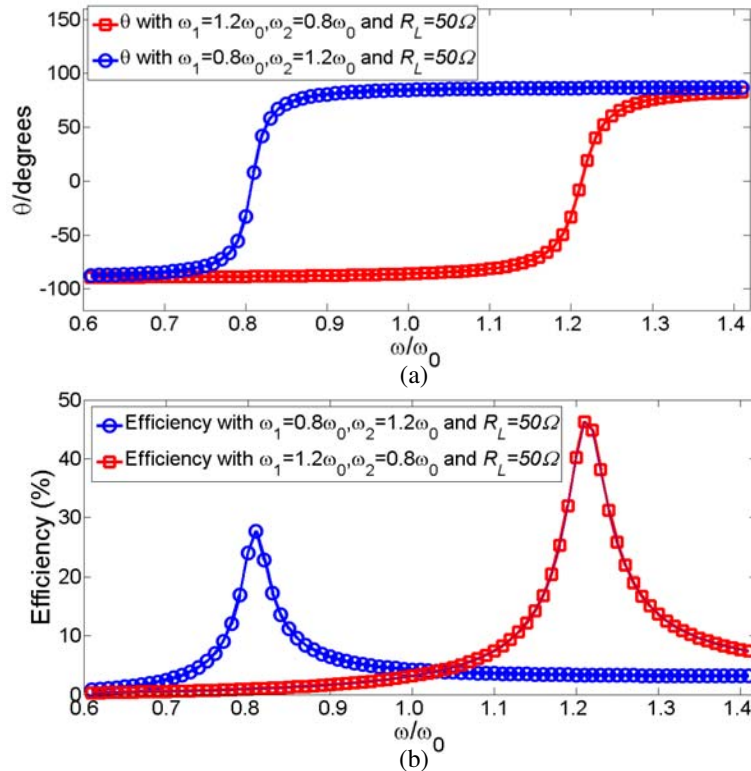


Figure 3. Simulation results with using the method of adjusting frequency, (a) θ versus ω/ω_0 . (b) Efficiencies versus ω/ω_0 .

The WPT system can operate at the resonant state by using the method of adjusting the operating frequency. θ is equal to zero at the new resonant frequency according to Eq. (9). The efficiency is improved according to Eq. (5). It can be seen from Fig. 3(a) that the new resonant angular frequency is $0.80\omega_0$ with $\omega_1 = 0.8\omega_0$, $\omega_2 = 1.2\omega_0$ and $R_L = 50\Omega$; whereas the new resonant angular frequency is $1.20\omega_0$ with $\omega_1 = 1.2\omega_0$, $\omega_2 = 0.8\omega_0$ and $R_L = 50\Omega$. The efficiency is very low at the original resonant angular frequency, whereas the efficiency can be improved at the new resonant angular frequency. Fig. 3(b) shows efficiency versus ω/ω_0 profiles for different combinations of ω_1 and ω_2 . It may be observed that the efficiency is 27.8% with $\omega = 0.80\omega_0$, $\omega_1 = 0.8\omega_0$ and $\omega_2 = 1.2\omega_0$, and the efficiency is 46.8% with $\omega = 1.20\omega_0$, $\omega_1 = 1.2\omega_0$ and $\omega_2 = 0.8\omega_0$.

4. PROPOSED METHOD

4.1. Analysis of the Effects of Frequency and Load Resistor on Efficiencies

The efficiency can be improved by adjusting the operating frequency when the resonant frequency drift occurs. However, the efficiency is still low. For example, the efficiency is 27.8% with $\omega_1 = 0.8\omega_0$, $\omega_2 = 1.2\omega_0$ and $R_L = 50\Omega$, and the efficiency is 46.8% with $\omega_1 = 1.2\omega_0$, $\omega_2 = 0.8\omega_0$ and $R_L = 50\Omega$. In this section, the method of coordinating the operating angular frequency and the load resistor is proposed in order to further improve efficiency.

According to Eq. (10), the resonant angular frequencies are related to the angular frequency of the transmission resonant coil ω_1 , the angular frequency of the receiving resonant coil ω_2 and the load resistor R_L . The efficiency is dependent on the resonant angular frequencies, ω_1 , ω_2 and R_L according to Eq. (5). The resonant frequencies can be calculated by using Eq. (10), then the efficiencies can be obtained according to Eq. (5). Table 2 to Table 5 show calculated efficiencies and resonant frequencies for different load resistors, ω_1 and ω_2 . It can be seen that the resonant frequency is changed as the load resistors ω_1 and ω_2 are changed. The efficiency is also changed as the load resistor and resonant frequencies are changed.

Table 2. Efficiencies and Resonant Frequency with $\omega_1 = 0.8\omega_0$ and $\omega_2 = 1.2\omega_0$.

R_L/Ω	$\omega_{RES,1}/\text{kHz}$	$\eta_{-1} (\%)$	$\omega_{RES,2}/\text{kHz}$	$\eta_{-2} (\%)$	$\omega_{RES,3}/\text{kHz}$	$\eta_{-3} (\%)$
0.6	123.2	59.3	121.3	58.4	78.6	3.34
1	\times^a	\times	\times	\times	78.6	5.45
2	\times	\times	\times	\times	78.6	10.2
5	\times	\times	\times	\times	78.7	20.9
10	\times	\times	\times	\times	78.8	30.7
20	\times	\times	\times	\times	79.3	35.5
30	\times	\times	\times	\times	79.5	33.7
40	\times	\times	\times	\times	79.7	30.7
50	\times	\times	\times	\times	79.8	27.8

$\omega_{RES,m}$ ($m = 1, 2, 3$) are resonant angular frequencies.
 η_{-m} ($m = 1, 2, 3$) are efficiencies at $\omega_{RES,m}$ ($m = 1, 2, 3$), respectively.
^a ‘ \times ’ is denoted as no value.

Table 2 shows calculated efficiencies and resonant frequencies with $\omega_1 = 0.8\omega_0$ and $\omega_2 = 1.2\omega_0$. Resonant frequencies are equal to 123.2 kHz, 121.3 kHz and 78.6 kHz with $R_L = 0.6\Omega$, respectively. However, there is only a resonant frequency for a given load resistor, which is varied from 1Ω to 50Ω . It can be seen that the resonant frequency is varied from 78.6 kHz to 79.8 kHz when the load resistor is varied from 1Ω to 50Ω . The efficiency is also changed as the load resistor and resonant frequencies are changed. The maximum efficiency is 59.3%; the resonant frequency is equal to 123.2 kHz; and the load resistor is 0.6Ω at the maximum efficiency point.

Table 3. Efficiencies and resonant frequency with $\omega_1 = 0.9\omega_0$ and $\omega_2 = 1.1\omega_0$.

R_L/Ω	$\omega_{\text{RES}_1}/\text{kHz}$	η_{-1} (%)	$\omega_{\text{RES}_2}/\text{kHz}$	η_{-2} (%)	$\omega_{\text{RES}_3}/\text{kHz}$	η_{-3} (%)
0.6	115.9	56.1	110.8	61.4	86.7	13.6
1	114.1	68.3	112.5	69.1	86.8	20.7
2	\times^a	\times	\times	\times	86.9	24.1
5	\times	\times	\times	\times	87.3	50.9
10	\times	\times	\times	\times	88.3	57.3
20	\times	\times	\times	\times	89.3	52.5
30	\times	\times	\times	\times	89.7	45.9
40	\times	\times	\times	\times	89.8	40.3
50	\times	\times	\times	\times	89.9	35.8

ω_{RES_m} ($m = 1, 2, 3$) are resonant angular frequencies.
 η_{-m} ($m = 1, 2, 3$) are efficiencies at ω_{RES_m} ($m = 1, 2, 3$), respectively.
^a ' \times ' is denoted as no value.

Table 3 shows calculated efficiencies and resonant frequencies with $\omega_1 = 0.9\omega_0$ and $\omega_2 = 1.1\omega_0$. Resonant frequencies are equal to 115.9 kHz, 110.8 kHz, and 86.7 kHz with $R_L = 0.6\Omega$, respectively. Resonant frequencies are equal to 114.1 kHz, 112.5 kHz, and 86.8 kHz with $R_L = 1\Omega$, respectively. However, there is only a resonant frequency for a given load resistor, which is varied from 2Ω to 50Ω . It can be seen that the resonant frequency is varied from 86.9 kHz to 89.9 kHz when the load resistor is varied from 2Ω to 50Ω . The efficiency is also changed as the load resistor and resonant frequencies are changed. The maximum efficiency is 69.1%, the resonant frequency is equal to 112.5 kHz and the load resistor is 1Ω at the maximum efficiency point.

Table 4. Efficiencies and resonant frequency with $\omega_1 = 1.2\omega_0$ and $\omega_2 = 0.8\omega_0$.

R_L/Ω	Resonant frequencies/kHz	η (%)
0.6	125.4	13.7
1	124.2	20.7
2	124.1	33.2
5	124.1	51.6
10	123.4	60.3
20	121.5	60.1
30	120.7	55.3
40	120.4	50.0
50	120.1	46.8

Table 4 shows calculated efficiencies and resonant frequencies with $\omega_1 = 1.2\omega_0$ and $\omega_2 = 0.8\omega_0$. There is only a resonant frequency for a given load resistor, which is varied from 0.6Ω to 50Ω . It can be seen that the resonant frequency is varied from 125.4 kHz to 120.1 kHz when the load resistor is varied from 0.6Ω to 50Ω . The efficiency is varied from 13.7% to 60.3% when the load resistor is varied from 0.6Ω to 10Ω . The efficiency is varied from 60.3% to 46.8% when the load resistor is varied from 10Ω to 50Ω .

Table 5 shows calculated efficiencies and resonant frequencies with $\omega_1 = 1.1\omega_0$ and $\omega_2 = 0.9\omega_0$. There is only a resonant frequency for a given load resistor, which is varied from 0.6Ω to 50Ω . It can be seen that the resonant frequency is varied from 116.8 kHz to 110.1 kHz when the load resistor is varied from 0.6Ω to 50Ω . The efficiency is varied from 24.0% to 69.0% when the load resistor is varied from

Table 5. Efficiencies and resonant frequency with $\omega_1 = 1.1\omega_0$ and $\omega_2 = 0.9\omega_0$.

R_L/Ω	Resonant frequencies/kHz	η (%)
0.6	116.8	24.0
1	116.7	33.9
2	116.4	49.1
5	115.0	65.3
10	112.5	69.0
20	110.8	62.8
30	110.3	55.7
40	110.2	50.0
50	110.1	45.1

0.6 Ω to 10 Ω . The efficiency is varied from 69.0% to 45.1% when the load resistor is varied from 10 Ω to 50 Ω .

4.2. Coordinating Frequency and Load Resistor Method

It is noted that the resonant frequency can be changed with load resistor variations, and the efficiency can also be changed with the operating frequency and load resistor variations. Therefore, we propose a method of coordinating the operating frequency and the load resistor to improve efficiency. The process of the proposed coordinating method is as follows:

- 1) The load resistor is changed from 0.5 Ω to 100 Ω in a step of 0.1 Ω according to the condition of practical constraints. It is assumed that the resonant frequency of each coil is varied from $0.8\omega_0$ to $1.2\omega_0$ when external environment changes [3].
- 2) The resonant angular frequencies at a given load resistor can be obtained by solving Eq. (10).
- 3) The resonant angular frequencies at a given load resistor are substituted into Eq. (5). The efficiency at a given resonant angular frequency and load resistor can then be obtained.
- 4) Compared to the efficiency at a given resonant angular frequency and load resistor, the optimum efficiency is obtained.
- 5) According to the optimum efficiency, the optimum load resistor and the optimum resonant angular frequency can be obtained. The detailed optimization process is shown in Fig. 4.

Using the proposed method, the simulation results are shown in Fig. 5 and Fig. 6. Fig. 5(a) shows the input impedance characteristic angle (θ) versus ω/ω_0 profiles for different combinations of ω_1 and ω_2 . It can be seen that resonant angular frequencies are equal to $0.79\omega_0$, $1.22\omega_0$, and $1.23\omega_0$ with $\omega_1 = 0.8\omega_0$ and $\omega_2 = 1.2\omega_0$, respectively. And the resonant angular frequency is equal to $1.22\omega_0$ with $\omega_1 = 1.2\omega_0$ and $\omega_2 = 0.8\omega_0$, respectively. Fig. 6(a) shows the input impedance characteristic angle (θ) versus ω/ω_0 profiles for different combinations of ω_1 and ω_2 . It can be seen that resonant angular frequencies are equal to $0.87\omega_0$, $1.13\omega_0$, and $1.14\omega_0$ with $\omega_1 = 0.9\omega_0$ and $\omega_2 = 1.1\omega_0$, respectively. And the resonant angular frequency is equal to $1.13\omega_0$ with $\omega_1 = 1.1\omega_0$ and $\omega_2 = 0.9\omega_0$, respectively. Simulation results of the resonant angular frequencies are the same as calculation results of Eq. (10). Fig. 5(b) shows efficiency versus ω/ω_0 profiles for different combinations of ω_1 and ω_2 . It may be observed that the efficiency is 63.6% with $\omega = 1.22\omega_0$, $\omega_1 = 0.8\omega_0$, and $\omega_2 = 1.2\omega_0$ and the efficiency is 63.1% with $\omega = 1.23\omega_0$, $\omega_1 = 0.8\omega_0$, and $\omega_2 = 1.2\omega_0$; whereas the efficiency is 4.3% with $\omega = 0.79\omega_0$, $\omega_1 = 0.8\omega_0$ and $\omega_2 = 1.2\omega_0$, and the efficiency is 63.0% with $\omega = 1.22\omega_0$, $\omega_1 = 1.2\omega_0$, and $\omega_2 = 0.8\omega_0$.

Figure 6(b) shows efficiency versus ω/ω_0 profiles for different combinations of ω_1 and ω_2 . It may be observed that the efficiency is 69.1% with $\omega = 1.13\omega_0$, $\omega_1 = 0.9\omega_0$ and $\omega_2 = 1.1\omega_0$, and the efficiency is 68.3% with $\omega = 1.14\omega_0$, $\omega_1 = 0.9\omega_0$ and $\omega_2 = 1.1\omega_0$; whereas the efficiency is 20.7% with $\omega = 0.87\omega_0$, $\omega_1 = 0.9\omega_0$, and $\omega_2 = 1.1\omega_0$, and the efficiency is 69.1% with $\omega = 1.13\omega_0$, $\omega_1 = 1.1\omega_0$ and $\omega_2 = 0.9\omega_0$. It is found that the resonant frequencies can be changed when the load resistor is changed, and the efficiencies are also changed when the load resistors and the resonant angular frequencies are changed.

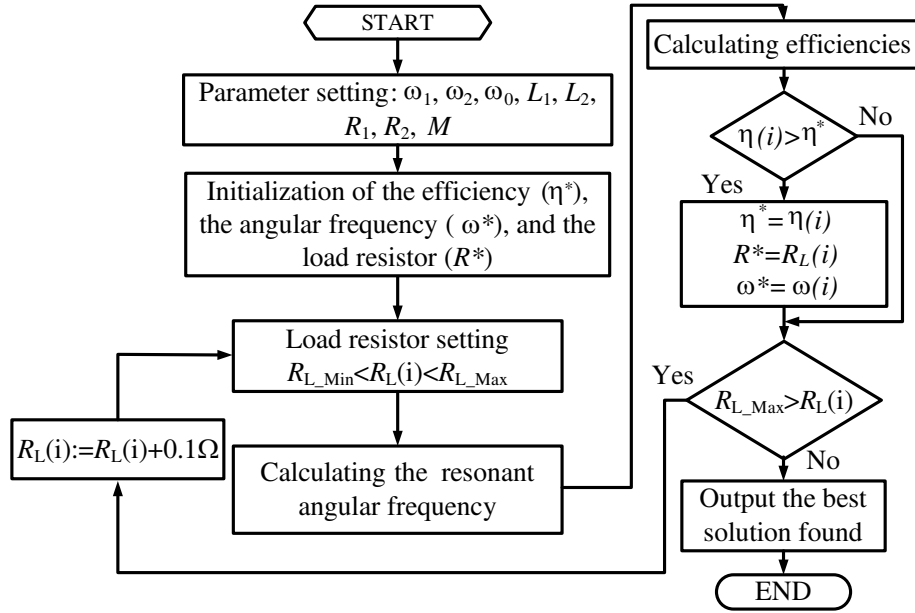


Figure 4. Flowchart of the optimization process by coordinating operating frequency and load resistor.

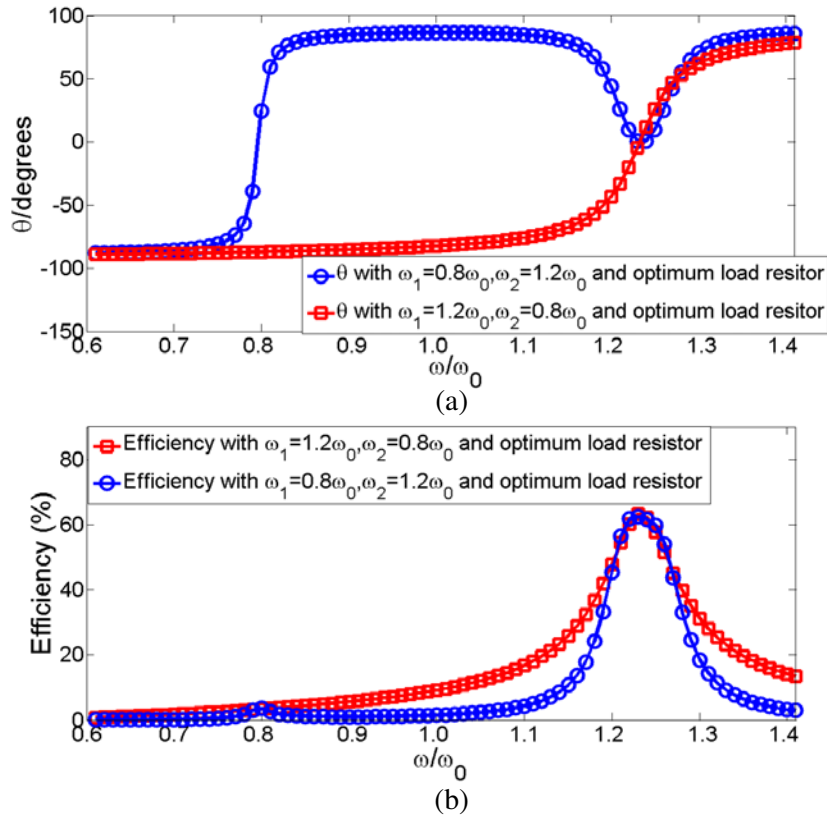


Figure 5. Simulation results with $\omega_1 = 1.2\omega_0, \omega_2 = 0.8\omega_0$ and $\omega_1 = 0.8\omega_0$ and $\omega_2 = 1.2\omega_0$. (a) θ versus ω/ω_0 . (b) Efficiencies versus ω/ω_0 .

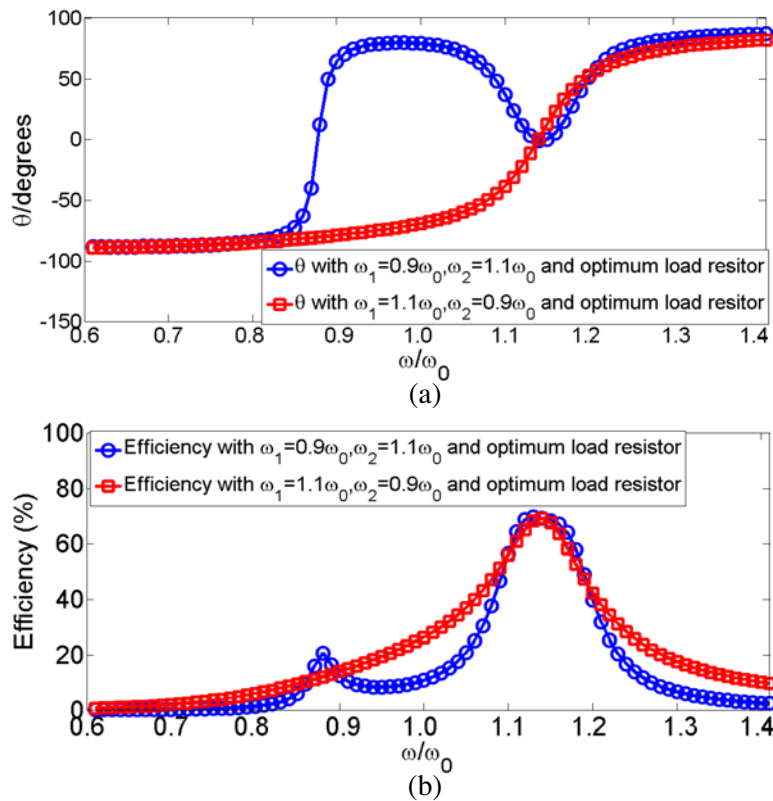


Figure 6. Simulation results with $\omega_1 = 1.1\omega_0$, $\omega_2 = 0.9\omega_0$ and $\omega_1 = 0.9\omega_0$, $\omega_2 = 1.1\omega_0$. (a) θ versus ω/ω_0 . (b) Efficiencies versus ω/ω_0 .

The optimum resonant angular frequency and the optimum efficiency can be obtained by using the proposed method.

5. MEASUREMENT RESULTS

5.1. The Experimental System

To validate the proposed method, the prototype model of the system has been built, as shown in Fig. 7. It is composed of the DC voltage source, two resonant coils, the quadruple-frequency inverter and the load. The value of the DC voltage source is 15 V, the fabricated DC voltage source is shown in Fig. 7(b). The two resonant coils are transmission and receiving coils. The transmission resonant coil is on the right. The receiving resonant coil is on the left, as shown in Fig. 7(c). The diameter of the transmission resonant coil is 40 cm with a pitch of 2 cm for approximately 6 turns. The parameters of the receiving resonant coil are the same as those of the transmission resonant coil. The parameters of the resonant coils can be calculated by using [29, 30]. An impedance analyzer TH2829A is used to extract the parameters in Eqs. (1) and (2). The original resonant frequency is set to be 100 kHz. The parameters of the resonant coils are listed in Table 6.

The quadruple-frequency inverter is used in this paper. Fig. 8 shows the schematic diagram of the inverter. The inverter consists of eight switch MOSFETs ($Q_1 \sim Q_8$) and two electrolytic capacitors (C_1 and C_2). IR2110 and IRF3205 are used as the gate driver and the switch MOSFET. The fabricated inverter is shown in Fig. 7(d). The inverter is controlled by the pulse-width-modulation (PWM) signals from the DXP28335 controller, as shown in Fig. 7(e). The inverter is suitable for working at high frequency (100 kHz–1 MHz).

D is set to 18 cm. The frequency of each resonant coil is changed by using high quality factor capacitances in order to simulate external environmental changes.

Table 6. Parameters of the resonant coils.

Symbol	Quantity	Value
L_1	the inductance of Tx	29.70 μH
L_2	the inductance of Rx	29.70 μH
C_1	the external compensating capacitance of Tx	85.28 nF
C_2	the external compensating capacitance of Rx	85.28 nF
R_1	the resistor of Tx	0.30 Ω
R_2	the resistor of Rx	0.29 Ω
f_0	the original resonant frequency	100.0 kHz

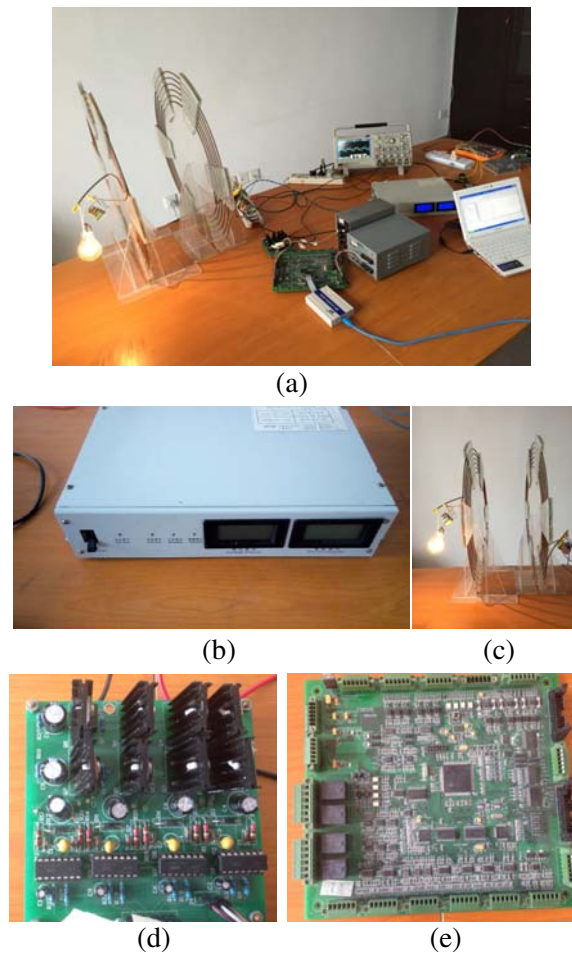


Figure 7. The experimental setup of the WPT system. (a) The overall experimental setup. (b) The DC voltage source. (c) The resonant coils. (d) The quadruple-frequency inverter. (e) The DXP28335 controller.

5.2. Adjusting the Operating Frequency

After replacing the bulb with a resistor, we firstly measure the system resonant frequencies and efficiencies by adjusting the operating frequency method. Fig. 9(a) shows the calculated and measured $\omega_{\text{RES}}/\omega_0$ profiles for different ω_1 (the system may have several resonant angular frequencies, the calculated and measured ω_{RES} is the resonant angular frequency at the maximum efficiency point,

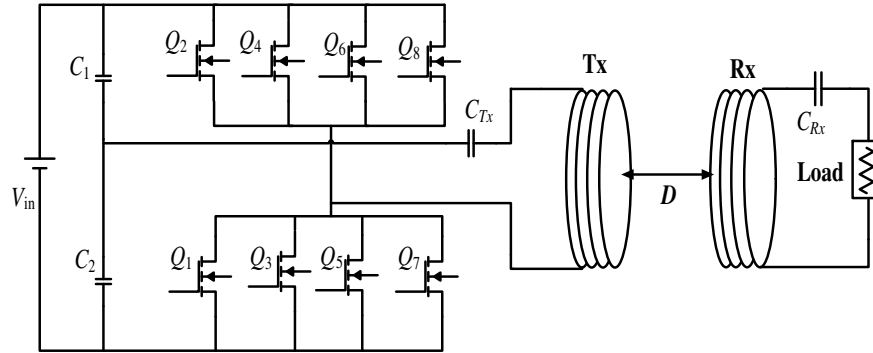


Figure 8. The schematic diagram of the inverter.

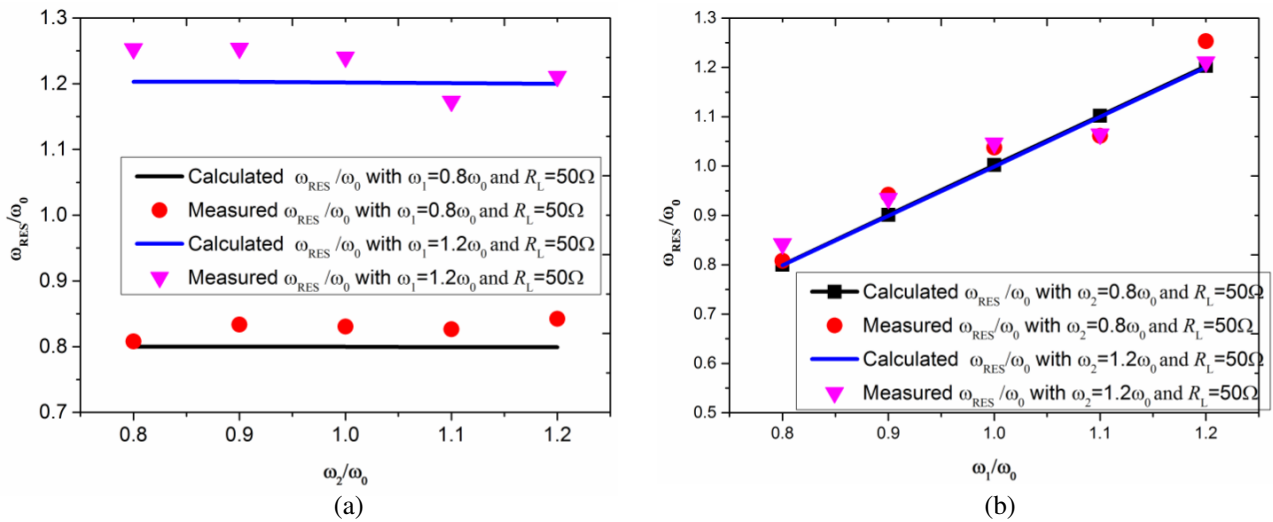


Figure 9. Measured and calculated results of ω_{RES}/ω_0 , (a) ω_{RES}/ω_0 versus ω_2/ω_0 for different ω_1 with $R_L = 50\Omega$. (b) ω_{RES}/ω_0 versus ω_1/ω_0 for different ω_2 with $R_L = 50\Omega$.

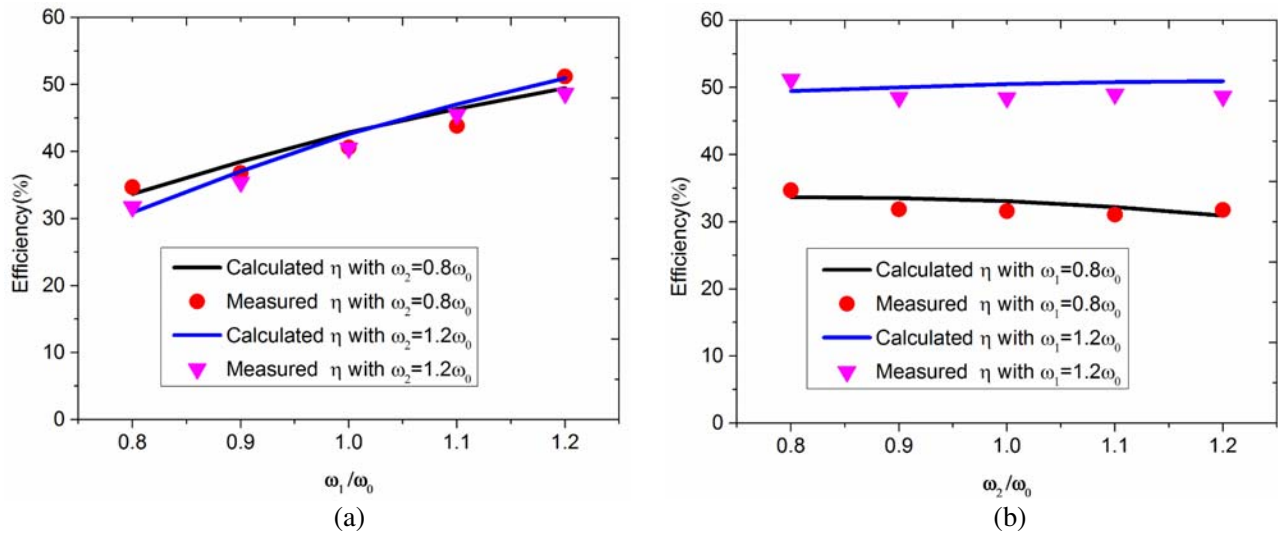


Figure 10. Measured and calculated results of efficiencies, (a) Efficiencies versus ω_1/ω_0 for different ω_2 with $R_L = 50\Omega$. (b) Efficiencies versus ω_2/ω_0 for different ω_1 with $R_L = 50\Omega$.

the following ω_{RES} is also the resonant angular frequency at the maximum efficiency point). It can be seen that $\omega_{\text{RES}}/\omega_0$ is nearly constant as the ω_2/ω_0 is varied from 0.8 to 1.2. $\omega_{\text{RES}}/\omega_0$ is nearly equal to 1.2 with $\omega_1 = 1.2\omega_0$ and $R_L = 50 \Omega$; whereas $\omega_{\text{RES}}/\omega_0$ is nearly equal to 0.8 with $\omega_1 = 0.8\omega_0$ and $R_L = 50 \Omega$.

Figure 9(b) shows the calculated and measured $\omega_{\text{RES}}/\omega_0$ profiles for different ω_2 . It can be seen that $\omega_{\text{RES}}/\omega_0$ is changed along with the change of ω_1/ω_0 . It is found that the resonant angular frequency ω_{RES} is determined by ω_1 with $R_L = 50 \Omega$. This is because the input impedance characteristic angle is equal to zero at $\omega = \omega_1$ in term of Eq. (9) even though the frequency of Rx deviates from the original resonant frequency. Fig. 10(a) shows the calculated and measured efficiencies versus ω_1/ω_0 profiles for different ω_2 . The efficiency is varied from 34.7% to 51.2% at $\omega_2 = 0.8\omega_0$ when ω_1/ω_0 is changed from 0.8 to 1.2. The efficiency is varied from 31.7% to 48.7% at $\omega_2 = 1.2\omega_0$ when ω_1/ω_0 is changed from 0.8 to 1.2. Fig. 10(b) shows the calculated and measured efficiencies versus ω_2/ω_0 profiles for different ω_1 . The efficiency is nearly constant for different ω_1 as ω_2/ω_0 is changed from 0.8 to 1.2. The efficiency is nearly equal to 32% at $\omega_1 = 0.8\omega_0$; whereas the efficiency is nearly equal to 49% at $\omega_1 = 1.2\omega_0$.

5.3. The Proposed Method

When the proposed method is used, Fig. 11(a) shows the calculated and measured optimum R_L versus ω_2/ω_0 profiles for different ω_1 . It can be seen that optimum R_L is changed as ω_2/ω_0 is varied.

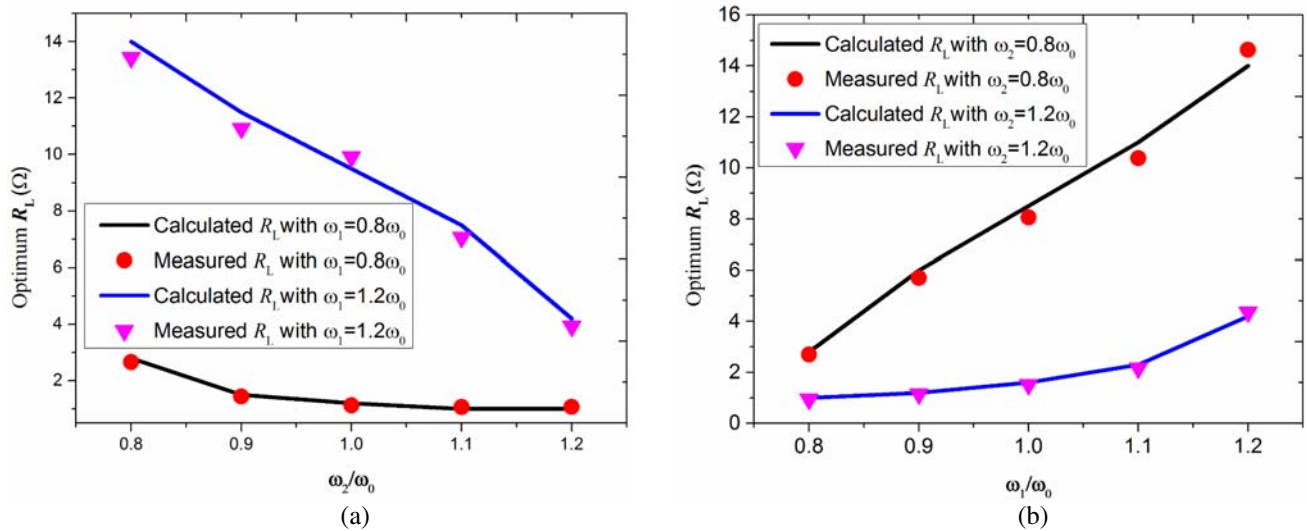


Figure 11. Measured and calculated results of optimum R_L , (a) Optimum R_L versus ω_2/ω_0 for different ω_1 . (b) Optimum R_L versus ω_1/ω_0 for different ω_2 .

Figure 11(b) shows the calculated and measured optimum R_L versus ω_1/ω_0 profiles for different ω_2 . It can also be seen that optimum R_L is also changed as ω_1/ω_0 is varied. There exists an optimum R_L for different combinations of ω , ω_1 , and ω_2 in order to obtain the optimum efficiency.

Figure 12(a) shows the calculated and measured optimum $\omega_{\text{RES}}/\omega_0$ versus ω_2/ω_0 profiles for different ω_1 . The optimum ω_{RES} is changed at $\omega_1 = 0.8\omega_0$ along with the change of ω_2 as ω_2/ω_0 is changed from 0.8 to 1.2; whereas the optimum ω_{RES} is nearly constant and equal to $1.2\omega_0$ with $\omega_1 = 1.2\omega_0$ as ω_2/ω_0 is changed from 0.8 to 1.2. Fig. 12(b) shows the calculated and measured optimum $\omega_{\text{RES}}/\omega_0$ versus ω_1/ω_0 profiles for different ω_2 . The optimum ω_{RES} is changed at $\omega_2 = 0.8\omega_0$ as ω_1/ω_0 is changed; whereas the optimum ω_{RES} is nearly constant with $\omega_2 = 1.2\omega_0$ as ω_1/ω_0 is changed from 0.8 to 1.2. It can be seen that ω_{RES} is changed along with the change of ω_1 when the method of adjusting the operating frequency is used, whereas the optimum ω_{RES} is determined by ω_1, ω_2 and the optimum load resistor R_L when the proposed method is used. This is because the resonant frequencies are changed with the load resistor variations in term of Eq. (10).

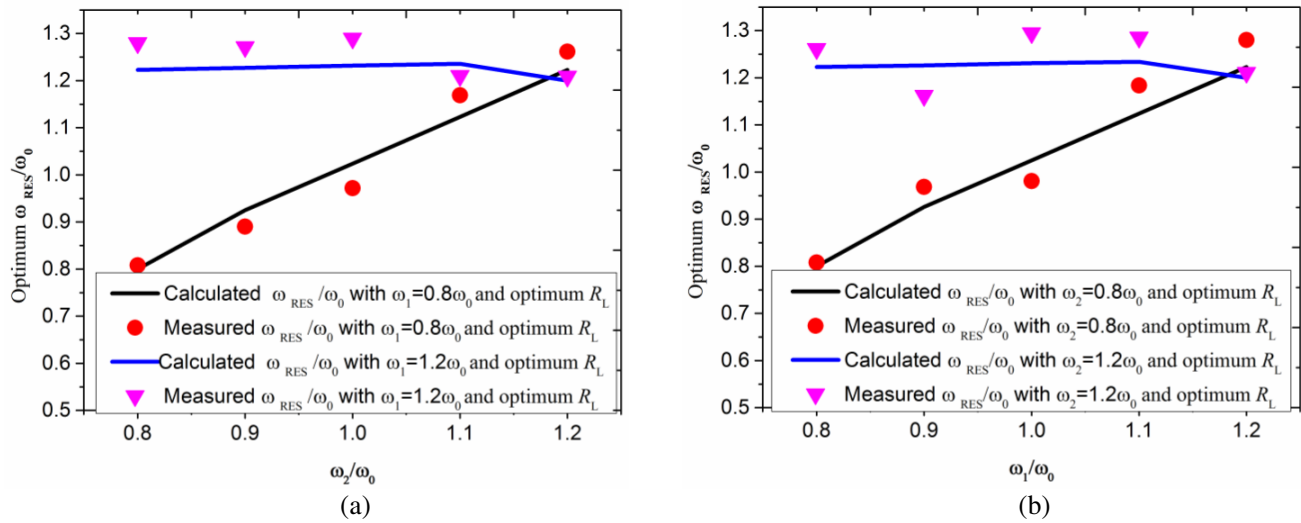


Figure 12. Measured and calculated results of optimum ω_{RES}/ω_0 , (a) Optimum ω_{RES}/ω_0 versus ω_2/ω_0 for different ω_1 with optimum R_L . (b) Optimum ω_{RES}/ω_0 versus ω_1/ω_0 for different ω_2 with optimum R_L .

When the optimum ω_{RES} and optimum load resistor are used, Fig. 13(a) shows the calculated and measured efficiencies versus ω_2/ω_0 profiles for different ω_1 . The efficiency is varied from 68.9% to 62.5% with $\omega_1 = 0.8\omega_0$ as ω_2/ω_0 is changed from 0.8 to 1.2. The efficiency is varied from 64.2% to 71.8% with $\omega_1 = 1.2\omega_0$ as ω_2/ω_0 is changed from 0.8 to 1.2. Fig. 13(b) shows the calculated and measured efficiencies versus ω_1/ω_0 profiles for different ω_2 . The minimum efficiency is 64.2% with $\omega_1 = 0.8\omega_0$ as ω_2/ω_0 is changed from 0.8 to 1.2. The minimum efficiency is 62.5% with $\omega_1 = 1.2\omega_0$ as ω_2/ω_0 is changed from 0.8 to 1.2. Compared with the method of only adjusting the operating frequency, the efficiency is improved by the proposed method. In this paper, the quality factors of Tx and Rx are not high. Therefore, the system efficiency is not high. However, the validity of the proposed method is not affected by this low efficiency. This paper focuses on optimization of efficiency under frequency drift.

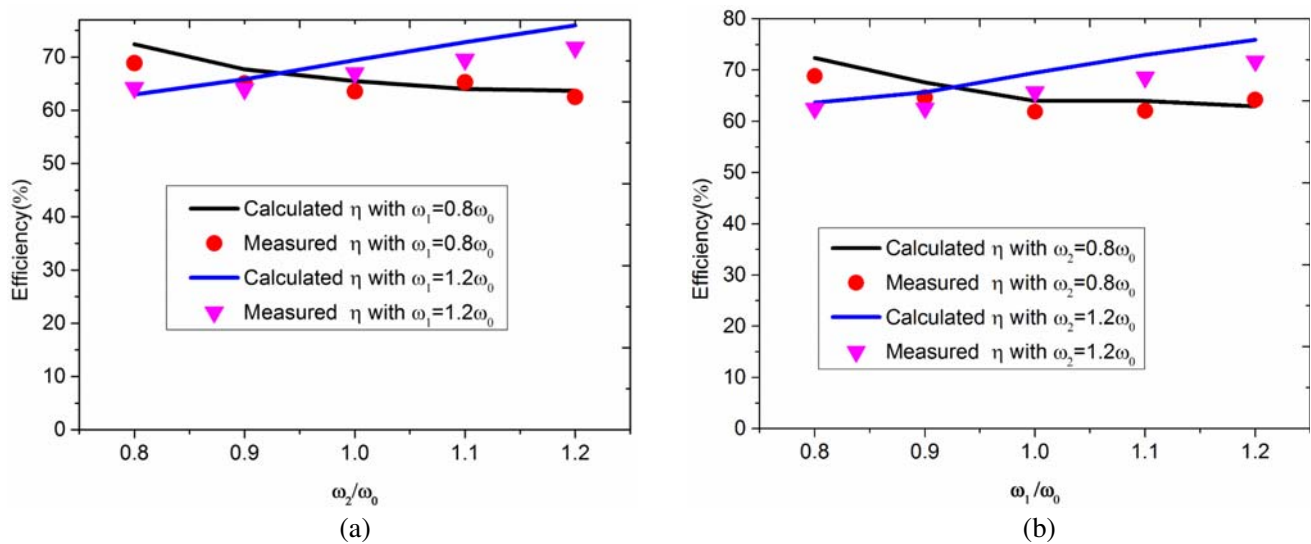


Figure 13. Measured and calculated results of efficiencies, (a) Efficiencies versus ω_2/ω_0 for different ω_1 with optimum R_L . (b) Efficiencies versus ω_1/ω_0 for different ω_2 with optimum R_L .

In the laboratory demonstration, the load resistor and the operating frequency are changed manually. However, the equivalent load resistor can be automatically changed by using impedance matching network [31]. The operating frequency can also be automatically changed by adjusting the switch frequency of the inverter in practical applications.

6. CONCLUSION

In this paper, a method of coordinating the operating frequency and the load resistor is presented to improve the efficiency when the resonant frequency drift occurs. Compared with the traditional adjusting operating frequency method, the efficiency is higher by using the proposed method. As examples, the maximum achievable efficiency is 51.2% by using the traditional method, whereas the efficiency is varied from 62.5% to 71.8% by using the proposed method. The efficiency is improved by using the proposed method.

Two key points are obtained in this paper. First, the load resistor variations will change the resonant frequency of the WPT system. Secondly, there may be several resonant frequencies. However, there is only an optimum resonant frequency to obtain the maximum efficiency. The proposed method is helpful for the design of frequency tracking technology. Future direction of this work is to introduce a method of parameter identification (L , C , and R) to estimate resonant frequency of each coil and to make the system more robust.

ACKNOWLEDGMENT

This work was supported in part by the National Natural Science Foundation of China under Grant 61104088 and 51377001, in part by the Hunan Provincial Department of Education under Grant 17C0469, in part by Hunan Provincial Natural Science Foundation of China under Grant 2018JJ3127, in part by Zhuzhou City Natural Science Foundation of China.

REFERENCES

1. Parise, M. and G. Antonini, "On the inductive coupling between two parallel thin-wire circular loop antennas," *IEEE Transactions on Electromagnetic Compatibility*, Vol. 60, No. 6, 1865–1872, 2018.
2. Shinohara, N., "The wireless power transmission: inductive coupling, radio wave, and resonance coupling," *Wiley Interdisciplinary Reviews-Energy and Environment*, Vol. 1, No. 3, 337–346, 2012.
3. Kurs, A., A. Karalis, R. Moffatt, et al., "Wireless power transfer via strongly coupled magnetic resonances," *Science*, Vol. 317, No. 6, 83–86, 2007.
4. Karalis, A., J. D. Joannopoulos, and M. Soljačić, "Efficient wireless non-radiative mid-range energy transfer," *Annals of Physics*, Vol. 323, No. 1, 34–48, 2008.
5. Hamam, R. E., A. Karalis, J. Joannopoulos, et al., "Efficient weakly-radiative wireless energy transfer: An EIT-like approach," *Annals of Physics*, Vol. 324, No. 8, 1783–1795, 2009.
6. Jaegue, S., S. Seungyong, K. Yangsu, et al., "Design and implementation of shaped magnetic-resonance-based wireless power transfer system for roadway-powered moving electric vehicles," *IEEE Transactions on Industrial Electronics*, Vol. 61, No. 3, 1179–1192, 2014.
7. RamRakhyani, A. K., S. Mirabbasi, and M. Chiao, "Design and optimization of resonance-based efficient wireless power delivery systems for biomedical implants," *IEEE Transactions on Biomedical Circuits and Systems*, Vol. 5, No. 1, 48–63, 2011.
8. Choi, S. Y., B. W. Gu, S. W. Lee, et al., "Generalized active EMF cancel methods for wireless electric vehicles," *IEEE Transactions on Power Electronics*, Vol. 29, No. 11, 5770–5783, 2014.
9. Chen, L., S. Liu, Y. Zhou, et al., "An optimizable circuit structure for high-efficiency wireless power transfer," *IEEE Transactions on Industrial Electronics*, Vol. 6, No. 1, 339–349, 2013.

10. Cheon, S., Y.-H. Kim, S.-Y. Kang, et al., "Circuit-model-based analysis of a wireless energy-transfer system via coupled magnetic resonances," *IEEE Transactions on Industrial Electronics*, Vol. 58, No. 7, 2906–2914, 2011.
11. Jinwook, D. K. and Y. Park, "Analysis of capacitive impedance matching networks for simultaneous wireless power transfer to multiple devices," *IEEE Transactions on Industrial Electronics*, Vol. 62, No. 5, 2807–2813, 2014.
12. Dukju, A. and H. Songcheol, "A transmitter or a receiver consisting of two strongly coupled resonators for enhanced resonant coupling in wireless power transfer," *IEEE Transactions on Industrial Electronics*, Vol. 61, No. 3, 1193–1203, 2014.
13. Dukju, A. and H. Songcheol, "A study on magnetic field repeater in wireless power transfer," *IEEE Transactions on Industrial Electronics*, Vol. 60, No. 1, 360–371, 2013.
14. Kiani, M., U.-M. Jow, and M. Ghovanloo, "Design and optimization of a 3-coil inductive link for efficient wireless power transmission," *IEEE Transactions on Biomedical Circuits and Systems*, Vol. 5, No. 6, 579–591, 2011.
15. Kim, J., H.-C. Son, K.-H. Kim, et al., "Efficiency analysis of magnetic resonance wireless power transfer with intermediate resonant coil," *IEEE Antennas and Wireless Propagation Letters*, Vol. 10, 389–392, 2011.
16. Lee, C. K., W. Zhong, and S. Hui, "Effects of magnetic coupling of nonadjacent resonators on wireless power domino-resonator systems," *IEEE Transactions on Power Electronics*, Vol. 27, No. 4, 1905–1916, 2012.
17. Huang, S. D., Z. Q. Li, and Y. Li, "Transfer efficiency analysis of magnetic resonance wireless power transfer with intermediate resonant coil," *Journal of Applied Physics*, Vol. 115, No. 17, 1–3, 2014.
18. Casanova, J. J., Z. N. Low, and J. S. Lin, "A loosely coupled planar wireless power system for multiple receivers," *IEEE Transactions on Industrial Electronics*, Vol. 56, No. 8, 3060–3068, 2009.
19. Xiu, Z., S. L. Ho, and W. N. Fu, "Quantitative analysis of a wireless power transfer cell with planar spiral structures," *IEEE Transactions on Magnetics*, Vol. 47, No. 10, 3200–3203, 2011.
20. Yang, Z., L. Wentai, and E. Basham, "Inductor modeling in wireless links for implantable electronics," *IEEE Transactions on Magnetics*, Vol. 43, No. 10, 3851–3860, 2007.
21. Kim, N. Y., K. Y. Kim, J. Choi, et al., "Adaptive frequency with power-level tracking system for efficient magnetic resonance wireless power transfer," *Electronics Letters*, Vol. 48, No. 8, 452–454, 2012.
22. Sample, A. P., D. A. Meyer, and J. R. Smith, "Analysis, experimental results, and range adaptation of magnetically coupled resonators for wireless power transfer," *IEEE Transactions on Industrial Electronics*, Vol. 58, No. 2, 544–554, 2011.
23. Duong, T. P. and J.-W. Lee, "Experimental results of high-efficiency resonant coupling wireless power transfer using a variable coupling method," *IEEE Microwave and Wireless Components Letters*, Vol. 21, No. 8, 442–444, 2011.
24. Juseop, L., L. Yong-Seok, Y. Woo-Jin, et al., "Wireless power transfer system adaptive to change in coil separation," *IEEE Transactions on Antennas and Propagation*, Vol. 62, No. 2, 889–897, 2014.
25. Minfan, F., Y. He, Z. Xinen, et al., "Analysis and tracking of optimal load in wireless power transfer systems," *IEEE Transactions on Power Electronics*, Vol. 30, No. 7, 3952–3963, 2015.
26. Yongseok, L., T. Hoyoung, L. Seungok, et al., "An adaptive impedance-matching network based on a novel capacitor matrix for wireless power transfer," *IEEE Transactions on Power Electronics*, Vol. 29, No. 8, 4403–4413, 2014.
27. Teck Chuan, B., M. Kato, T. Imura, et al., "Automated impedance matching system for robust wireless power transfer via magnetic resonance coupling," *IEEE Transactions on Industrial Electronics*, Vol. 60, No. 9, 3689–3698, 2013.
28. Dukju, A. and H. Songcheol, "A study on magnetic field repeater in wireless power transfer," *IEEE Transactions on Industrial Electronics*, Vol. 60, No. 1, 360–371, 2013.

29. Khan, S. R., S. K. Pavuluri, and M. P. Y. Desmulliez, “Accurate modeling of coil inductance for near-field wireless power transfer,” *IEEE Transactions on Microwave Theory and Techniques*, Vol. 66, No. 9, 4158–4169, 2018.
30. Ke, Q., W. Luo, G. Yan, et al., “Analytical model and optimized design of power transmitting coil for inductively coupled endoscope robot,” *IEEE Transactions on Biomedical Engineering*, Vol. 63, No. 4, 694–706, 2016.
31. Zhong, W. X. and S. Y. R. Hui, “Maximum energy efficiency tracking for wireless power transfer systems,” *IEEE Transactions on Power Electronics*, Vol. 30, No. 7, 4025–4034, 2015.